* Revised Manuscript (including Abstract)
ACCEPTED MANUSCRIPT

# Passivation Behavior of Type 304 Stainless Steel in A Non-aqueous Alkyl Carbonate Solution Containing $LiPF_6$ Salt

Seung-Taek Myung,[a,*] Yusuke Sasaki,[a] Takamitsu Saito,[b] Yang-Kook Sun,[c] Hitoshi Yashiro[a,*]

[a]*Department of Chemical Engineering, Iwate University, 4-3-5 Ueda, Morioka, Iwate 020-8551, Japan*

[b]*Nissan Motors, 1 Natsushima, Yokosuka, Kanagawa 273-8523, Japan*

[c]*Department of Chemical Engineering, Hanyang University, Seungdong-Gu, Seoul 133-791, South Korea*

## *Abstract*

Passivation behavior of type 304 stainless steel in a non-aqueous alkyl carbonate solution containing $LiPF_6$ salt was studied using electrochemical polarization, X-ray photoelectron spectroscopy (XPS) and time of flight – secondary ion mass spectroscopy (ToF-SIMS). Cathodic polarization to 0 V vs. $Li/Li^+$ resulted in most but not complete reduction of the air-formed film from oxides to metal on the stainless steel, as

*Corresponding author
Tel/fax: +81-19-621-6330
E-mail: yashiro@iwate-u.ac.jp
Tel/fax: +81-19-621-6345
E-mail: smyung@iwate-u.ac.jp



Accepted Manuscript

ACCEPTED MANUSCRIPT

confirmed by XPS. For complete elimination of the air-formed film, the surface of the stainless steel was scratched under anodic polarization conditions. At 3 V vs. $Li/Li^+$ where an anodic current peak appeared, only an indistinct layer was recognized on the newly scratched surface, according to ToF-SIMS analysis. Above 4 V vs. $Li/Li^+$, substantial passive films were formed, which were composed of oxides and fluorides of iron and chromium. The origin of oxide was due to water contained in the non-aqueous alkyl carbonate solution, and that of fluorides were the result of the decomposition of electrolytic salt, $LiPF_6$, especially at higher potential. The resultant passive films were stable in the non-aqueous alkyl carbonate solution containing $LiPF_6$ salt.

*Keywords*; Type 304; Stainless steel; Scratch; Non-aqueous solution; Passive film; Corrosion resistance; ToF-SIMS

## *1. Introduction*

Stainless steels have been widely used because their air-formed films based on (Cr, Fe) oxides on the surface protect the metal bulk from general corrosion. The passivation mechanism of stainless steels in aqueous solutions has been extensively



Accepted Manuscript

ACCEPTED MANUSCRIPT

studied [1-3]. Passive films are believed to be oxides/hydroxides containing water molecules, especially when formed in aqueous solution. Cathodic polarization treatments are commonly adopted prior to anodic polarization in order to approximate the surface to a bare state although all of these oxide films could not be reduced to meals in aqueous solutions. Increasing the potential causes active dissolution of the metal ingredients to form (Cr, Fe) oxides on the surfaces of metal bulk. The resulting oxide layer is the passivation film. Fe-oxides are selectively soluble at lower pH so that Cr-oxides are the major constituent of the film. Alternatively, Cr-oxides are preferentially dissolved at higher pH and potential, and the outer layer of the stainless steel is mainly composed of an Fe-oxide layer. Passivation in such a manner provides a significant corrosion resistance to stainless steel. However, most non-aqueous organic solutions will not allow passivation this way due to lack of water molecules in the electrolyte.

A good example of metal passivation in an anhydrous solution is in lithium batteries. Lithium batteries are completely sealed in compact housings to avoid contact with water molecules that detrimentally effect battery performance. In the system, electroactive materials are coated to metallic foil current collectors. The current collector should be electrochemically stable in contact with cell components over the





Accepted Manuscript

ACCEPTED MANUSCRIPT

operation potential window of used electrodes. Therefore, Al foil is widely used as the current collector for lithium battery applications since the air-formed oxide, $Al_2O_3$, of Al passivates well in $LiPF_6$, $LiClO_4$, and $LiBF_4$-containing alkyl carbonate solutions [4-7].

There remains a lack of information on the passivity of metals in organic and mixed aqueous/non-aqueous solutions. In 1974, Heitz reviewed the state of the understanding of the corrosion of metals and alloys in organic solvents [8]. Kurger et al. [9-12] observed that type 304 stainless steel readily passivated up to 4.9 V vs. $Li/Li^+$ in $LiClO_4$/PC, even though the detailed passivation mechanism was not clarified. Komaba et al. [13] evaluated a positive electrode material by applying $LiMn_2O_4$ active material on a stainless steel current collector. Stainless steels are still being employed as cell cases with uncertain chemistries. In this study, passivation process of type 304 in a non-aqueous alkyl carbonate solution containing $LiPF_6$ salt as an electrolyte is reported.

## *2. Experimental*

To follow the electrochemical behavior of commercial type 304 stainless steel foil with10 μm thickness in $LiPF_6$ contained alkyl carbonate solution, Al pouch cells were fabricated in an Ar-filled glove box. The nominal chemical composition of the type 304 stainless steel is described in Table 1. The stainless steel foil was used as





Accepted Manuscript

ACCEPTED MANUSCRIPT

received. Prior to use, the specimen surface was cleaned ultrasonically in acetone. The electrochemical cells consisted of the stainless steel foil (0.283 $cm^2$) as a working electrode and lithium metal sheets as counter and reference electrodes were separated by a porous polypropylene separator, where 1 M $LiPF_6$ in ethylene carbonate (EC) – dimethyl carbonate mixture (DMC) (1:1 ratio by volume) was contained as an electrolyte.

Two methods were used to study the passivation behavior of the bare surface of the specimen. The first method used an electrochemical cell that was first cathodically polarized to 0 V vs. $Li/Li^+$ from an open circuit potential (OCP). The polarization was continued in the anodic direction up to 5 V vs. $Li/Li^+$ by sweeping 10 mV $s^{-1}$ at 40 $^oC$. The scanning was performed in triplicate.

The stainless steel foil polarized to 0 V vs. $Li/Li^+$ was rinsed with a salt-free DMC solution overnight in a glove box to remove residual $LiPF_6$ salt. The specimen was transferred to an X-ray photoelectron spectroscopy (XPS, ULVAC-PHI 5600) chamber without exposure to air. XPS analysis was performed with a monochromatic Al-K$\alpha$ source. The take-off angle of the emitted photoelectrons was typically adjusted to 45$^o$ with respect to the surface. The depth scale for sputtering was calibrated relative to the anodically formed $SiO_2$ standard layers. The sputter rate was determined to be 2.7





Accepted Manuscript

ACCEPTED MANUSCRIPT

nm $min^{-1}$ for the applied conditions of the Ar-ion gun. Values of binding energies of the XPS standard peaks reported in the available literatures were used in this study [14].

The second method used scratch in the surface of stainless steel foil under a polarized condition. Thus, the specimen was cathodically polarized to 0 V vs. $Li/Li^+$ from OCPs and then anodically polarized to 3, 4, and 5 V vs. $Li/Li^+$ by sweeping 10 mV $s^{-1}$ at 40 $^oC$. After reaching the potentials, the surface of the stainless steel electrode (disc, $\phi$ 8 mm) was briefly scratched by a diamond polishing tip rotating at 100 rpm in a specially designed PTFE cell (Fig. 1) in an Ar-filled box. After the scratch, polarizations were immediately performed at each potential for 300 seconds in a transient mode.

The scratched surfaces of the stainless steel after the polarization were examined by time-of-flight secondary ion mass spectroscopy (ToF-SIMS, ULVAC-PHI TFS2000, Perkin Elmer) at $10^{-9}$ Torr. The electrodes were washed with a salt-free DMC solution overnight in a glove box to remove the remaining $LiPF_6$ salt. This instrument was also equipped with a liquid $Ga^+$ ion source and pulse electron flooding. During analysis, the targets were bombarded by pulsed 15 keV $Ga^+$ beams. The total collection time was 1000 s over a 12 x 12 μm area.

## *3. Results and discussion*



Accepted Manuscript

ACCEPTED MANUSCRIPT

Figure 2 shows three consecutive cyclic voltammogram (CV) of type 304 stainless steel measured at 40 $^{o}$C. Polarization started for the cathodic direction from the open circuit potential (OCP). A cathodic peak between 1 and 2 V vs. Li/Li$^{+}$ is supposed as the reduction of the air-formed Fe and/or Cr-oxides films to metal, the electrolytic salt formation of $Li_2O$, and the formation of the solid electrolyte interfacial (SEI) layer [15]. Similar to the first cycle, the distinct cathodic peak at 1 V – 2 V vs. Li/Li$^{+}$ in the second cycle indicates that the anodically formed films were reduced almost to metals. A distinct cathodic peak near 0.5 – 0.7 V vs. Li/Li$^{+}$ could be assigned to the under potential deposition (UPD) of Li on the stainless steel surface. In the anodic direction, the anodic peak appearing at 1.1 V – 1.3 V vs. Li/Li$^{+}$ would result from the oxidation of the deposited Li. UPD and the corresponding oxidation of Li were also progressive at a lower potential, though the redox potential was slightly shifted. The magnitude of the current in the potential range of 0 – 2.0 V vs. Li/Li$^{+}$ decreased in the second cycle. Another anodic peak was observed at 2 V vs. Li/Li$^{+}$, which is assumed to be an oxidation process of Cr metals to oxides. However, the oxidation reaction was not apparent at the potential from the second cycle. In the range of 2.8 – 3.8 V vs. Li/Li$^{+}$ to the noble potential, a small anodic peak was observed due to the oxidation of $Fe^{0}$ and/or $Cr^{III}$. The corresponding reduction process was observed in the same potential range. A





Accepted Manuscript

ACCEPTED MANUSCRIPT

slightly increased anodic current was found at 2.8 V – 3.8 V vs. $Li/Li^+$ in the second cycle, and was slightly greater at the third cycle. This means that passive film of the stainless steel was formed at this potential. After the active dissolution, the anodic current was maintained at a very low level ($\leq$ 15 μA) up to 5 V vs. $Li/Li^+$ as shown in the inset of Fig. 2, implying that the passive films were further stabilized. No significant change appeared in the current near 5 V vs. $Li/Li^+$ during repetitive CV scanning. In fact, the air-formed surface film of type 304 stainless steel is composed of Fe- and Cr-oxides. The presence of oxide layers prevents the general corrosion of the stainless steel. From a thermodynamic consideration, however, Cr itself, which is one of the main elements of type 304 stainless steel, can be completely oxidized to hexavalent at 4.33 V vs. $Li/Li^+$ that is obtained by a simple conversion of the SHE potential (1.33 V vs. SHE [16]) to the potential versus Li metal. In this experiment, the used non-aqueous electrolyte contains a negligible amount of water, less than 50 ppm. Thus, the activity of water in the system is too small for transpassivation of $Cr^{III}$ to occur below 5 V vs. $Li/Li^+$. Based on the pH-potential map, those reactions may occur at a much higher potential [17]. However, due to the instability of electrolyte at higher potential, it was not possible to increase the potential higher than 5 V vs. $Li/Li^+$. The expected dissolution did not occur significantly to 5 V vs. $Li/Li^+$ in the non-aqueous electrolyte (Fig. 2), revealing that the





Accepted Manuscript

ACCEPTED MANUSCRIPT

stainless steel was well passivated in the $LiPF_6$-containing alkyl carbonates solution.

To follow the passivation of type 304 stainless steel, XPS measurements were performed using the polarized electrode to 0 V vs. $Li/Li^+$ from the OCP. Figure 3 shows the corresponding XPS spectra of Fe2p and Cr2p spectra after the cathodic polarization. In the as-polarized state, Fe metal and oxides peaks were seen in Fig. 3a. Due to the disturbance of the formed SEI film in the most outer surface, the chemical states of Fe and Cr elements after the polarization could not be clearly observed. For this reason, Ar-ion etching was done for two minutes to remove the SEI layer and/or air-contaminates during sampling. After etching, the Fe metal-related peak (707 eV) was primarily observed with a very small trace of $Fe^{III}$-oxide (711 eV), after which, there was no increase in the $Fe^{III}$-oxide as the etching time increased. For the Cr spectra in Fig. 3b, etching for two minutes resulted in the advent of Cr metal (574.4 eV) and $Cr^{III}$-oxide (577 eV), after which the reflection of Cr metal is getting stronger with increasing sputtering time. Even though the stainless steel electrode was reduced to 0 V vs. $Li/Li^+$, the presence of oxide peaks belonging to metal oxides ($Fe^{III}$-O and $Cr^{III}$-O) was still confirmed. It is likely that either the original air-formed layer was not completely eliminated or contact with air during the sample handling for the measurement may have elicited the negligible traces of oxides in Fig. 3.





Accepted Manuscript

ACCEPTED MANUSCRIPT

It was first hypothesized that if the air-formed layers were completely reduced to Fe and Cr metals through the cathodic polarization to 0 V vs. $Li/Li^+$, it would be possible to expect the passivation process of the metallic elements up to 5 V vs. $Li/Li^+$ . Unfortunately, the air-formed passive layer remained after the polarization. Thus, to form a new oxide-free new surface, the stainless steels were first cathodically polarized to 0 V vs. $Li/Li^+$ and anodically polarized to 3 V, 4 V, and 5 V vs. $Li/Li^+$ at 40 $^oC$. As soon as the potential reached the desired potentials, the remaining oxide passive layer was mechanically scratched using a diamond polishing tip with 100 rpm in a specially designed H-type cell at 40 $^oC$ (Fig. 1). It was assumed that the oxide layer was completely removed by the scratching, and the newly formed metallic surfaces were subsequently polarized in a transient mode for 300s at 40 $^oC$ in the H-type cell.

Figure 4 displays the results of current and time curves of the scratched electrodes polarized at 3 V, 4 V, and 5 V vs. $Li/Li^+$ at 40 $^oC$. The abrupt decay of current in the early state (within 30s) and retention of the current at a lower level during the polarization clearly indicates the formation and growth of a passive layer for all cases without critical defects that can be caused by corrosion on the scratched film. If the passive film was not stabilized, the resulting transient current should fluctuate or increase due to breakdown. After the fast decay of the transient current, the current



Accepted Manuscript

ACCEPTED MANUSCRIPT

retained at a very low level. This implies that as soon as the whole surface is well covered by the passive film, the current, which is necessary to maintain the passivation, becomes very low. However, it is difficult to compare the absolute value of the current depending on the potential because the scratched area of the electrode could not be controlled.

After the polarization in Fig. 4, the electrodes were analyzed with ToF-SIMS to follow the passivation. Since the groove possessing the newly formed passive layer is very narrow (~ 20 μm in Fig. 5a and b), XPS, which analyzes relatively a large area (400 μm x 400 μm), could not be employed for the measurement. This means that, the information on the unscratched part can be merged with the scratched part in spectra during measurement, if XPS is used. For this reason we used ToF-SIMS that is able to produce a small ion beam ($Ga^+$), less than (12 μm x 12 μm). Though quantitative analysis is difficult by ToF-SIMS, the technique has a very high sensitivity for the qualitative surface analysis of molecule ions detection, even though the analyzing area is very narrow. Figure 5a depicts a clear vestige of the scratch, and the resulting secondary ion mapping image of the polarized electrode at 3 V vs. $Li/Li^+$ is displayed in Fig. 5b. Figure 5b was obtained without bunching of the primary $Ga^+$ ions so that a clear image of secondary ions could be collected for the area (240 μm x 240 μm). For





Accepted Manuscript

ACCEPTED MANUSCRIPT

analysis, the raster size was focused to 12 μm x 12 μm and the center of the newly formed groove (marked by arrow) was investigated using bunched $Ga^+$ ions for better mass resolution. In the as-polarized region, some fragments of oxides and fluorides (such as $CrO^+$, $CrF^+$, $FeO^+$, and $FeF^+$) were detected, and the resulting intensities were weak less than 300 counts in Fig. 5c. No significant changes were observed, even after $Ga^+$ ions beam etching (240 μm x 240 μm) for 10s in Fig. 5d. Further etching by $Ga^+$ ions demonstrates that no other compounds remained on the new surface (Fig. 5e-g). As shown in the inset of Fig. 2, the rise of current indicates that active dissolution of metal elements was occurring at 3 vs. $Li/Li^+$. It is likely that the formed film might be thin and not well-organized in the potential range, as confirmed by ToF-SIMS.

As shown in Fig. 4, the scratched groove under polarization at 4 V vs. $Li/Li^+$ was also examined. The observed image of Fig. 6a coincides with that of Fig. 6b. The width of the scratched groove was approximately 20 μm. The electrode polarized at 4 V vs. $Li/Li^+$ showed a strong secondary ion intensity on the groove in Fig. 6b, which was different from the secondary ion mapping image of the polarized electrode at 3 V vs. $Li/Li^+$. As shown in Fig. 6d-f, etching for 10s resulted in a significant increase in the $CrF^+$ and $CrO^+$ fragments. On the other hand, the developments of $FeF^+$ and $FeO^+$ fragments were seemed to be slower in Fig. 6d-f than those of Cr-containing compounds.



Accepted Manuscript

ACCEPTED MANUSCRIPT

The $CrF^+$ fragment remained throughout the ToF-SIMS measurement in Fig. 6c-g. At the potential (4 V vs. $Li/Li^+$), the active dissolution of metal was already terminated near 3.8 V vs. $Li/Li^+$ so that the corresponding current stayed in a very low level approximately 7 $\mu A\ cm^{-2}$, as shown in the inset of Fig. 2. It is believed that the newly formed passive film is thick and well-constructed with two components, oxides and fluorides.

Investigation was also performed after the polarization at 5 V vs. $Li/Li^+$. The intensity of the secondary ions of the scratched parts was very high in Fig. 7b. Similar to 4 V vs. $Li/Li^+$, $CrO^+$, $CrF^+$, $FeO^+$, and $FeF^+$ fragments were strongly present in Fig. 7c. Interestingly, the intensity for the $FeO^+$, and $FeF^+$ fragments appeared much stronger at 5 V vs. $Li/Li^+$ in comparison with Fig. 6. $CrF^+$ and $FeF^+$ fragments were much intensified at 5 V vs. $Li/Li^+$ in Fig. 7f, although the $CrF^+$ shows a much higher intensity in Fig. 8b. It is clear that the new surface was well passivated with (Fe, Cr)-oxides and (Fe, Cr)-fluorides. The formation of those fluoride layers on the surface indicates that the newly formed surface experienced reactions with the $LiPF_6$-contained electrolyte.

In an OCP state, the outer surface of type 304 stainless was passivated with air-formed thin oxides layer, which protects general corrosion. Cathodic polarization to 0 V vs. $Li/Li^+$ from the OCP may result in the reduction of metal oxides to metals by the



Accepted Manuscript

ACCEPTED MANUSCRIPT

following reactions, as schemed in Fig. 9:

$$Cr_2O_3 + 6Li^+ + 6e^- \rightarrow 2Cr + 3Li_2O \qquad (1),$$

$$Fe_2O_3 + 6Li^+ + 6e^- \rightarrow 2Fe + 3Li_2O \qquad (2).$$

Accordingly, majority of the metallic peaks for the Cr and Fe was derived from the above reactions though small portions of oxides were remained in the XPS spectra of Fig. 3. Similar tendency was observed in the lithiated $Cr_2O_3$ thin film reported by Li et al. [18] With increasing potential, the anode peak associated with the active dissolution near 2.8 to 3.8 V vs. $Li/Li^+$ (Fig. 2) gave rise to the passivation of the stainless steel electrode. The passivation of the stainless steel was observed to be in progress at an intermediate potential of 3 V vs. $Li/Li^+$ and the resulting film was thin. The traces of metal-oxide fragments (Fig. 5) could be ascribed to the active dissolution of metal to oxide on the most outer surface:

$$2Cr + 3Li_2O \rightarrow Cr_2O_3 + 6Li^+ + 6e^- \qquad (3),$$

$$2Fe + 3Li_2O \rightarrow Fe_2O_3 + 6Li^+ + 6e^- \qquad (4).$$



Accepted Manuscript

ACCEPTED MANUSCRIPT

After completion of the active dissolution near 4 V vs. $Li/Li^+$, the appearances of strong fragments ($CrF^+$, $CrO^+$, $FeO^+$, and $FeF^+$) in Fig. 6 clearly demonstrated that the outer surface of the stainless steel was well constructed by those compounds on the metal bulk. In fact, $LiPF_6$-based electrolyte always contains a small amount of water, which consequently causes breakdown of the electrolyte accompanied by HF generation. Propagation of HF is also facilitated by increasing temperature (40 $^oC$ in this experiment) and water concentration. Thus, $LiPF_6$ electrolytic salt can be decomposed, and the reaction is accelerated at higher potentials and temperatures, according to the following reactions suggested by Aurbach et al. [19] and Edström et al.[20]:

$$LiPF_6 \rightarrow LiF + PF_5 \qquad (5),$$

$$PF_5 + H_2O \rightarrow POF_3 + 2HF \qquad (6).$$

Therefore, it is possible that the (Cr, Fe)-oxides components of the passive layer react with the generated HF into the electrolyte. Then, the byproducts would be detected as fragments with Fe-F and Cr-F bonding as seen in Figs. 6 and 7, assuming the following reactions:



Accepted Manuscript

ACCEPTED MANUSCRIPT

$$Cr_2O_3 + 6HF \rightarrow 2CrF_3 + 3H_2O \quad (7),$$

$$Fe_2O_3 + 6HF \rightarrow 2FeF_3 + 3H_2O \quad (8).$$

In Figs. 6f-g and Figs. 7f-g, the intensity ratios of $CrO^+$ versus $CrF^+$ and $FeO^+$ versus $FeF^+$ were getting higher by $Ga^+$ ions beam etching for 300s and 1000s supports that the oxide layers were located beneath the fluoride layer. Hence, it is believed that the outer passive oxides layer was slowly transformed to metal fluorides layer at higher potential (Fig. 9). Reactions shown in Equations (7) and (8) would be accelerated at 5 V vs. $Li/Li^+$ (Fig. 7) due to the formation of more amount of HF at higher potential in the electrolyte. For this reason, traces of $CrF^+$ and $FeF^+$ fragments appeared much stronger than at 4 V vs. $Li/Li^+$ in Fig. 7.

Myung et al. [21-23] proved with ToF-SIMS that amphoteric metal oxide surfaces were transformed to metal fluorides through the intermediate state of metal oxyfluorides after exposing those oxide materials into $LiPF_6$-containing electrolyte. Kanamura et al. [5] reported that an $AlF_3$ passive film was derived from an $Al_2O_3$ oxide layer on Al foil by anodic polarization to 6 V vs. $Li/Li^+$. Successful passivation achieved by the formation of $AlF_3$ on the $Al_2O_3$ surface of Al foil made it possible to be widely used as a current collector of positive electrode for lithium-ion batteries, where



Accepted Manuscript

ACCEPTED MANUSCRIPT

the Al foil is always exposed to HF contained in alkyl carbonates solution. Similar tendencies were also demonstrated, even in amphoteric oxide-coated electroactive positive electrode active materials for lithium batteries [21-27]. As the electrochemical cycling goes by, the outer surface of amphoteric oxides loaded on the surface of the active materials was slowly transformed to metal oxyfluoride and/or fluorides. The formed new layers sufficiently protect the electroactive materials from HF attack from the electrolyte during the electrochemical cyclings.

For the type 304 stainless steel, the formation of an alloy with Li metal near 0 V vs. $Li/Li^+$ in Fig. 2 was not observed. Furthermore, the presences of Fe-fluoride and Cr-fluoride on the surface of stainless steel also played an important role in passivating the stainless surface, and corrosion resistance, thereby, was significantly improved. As a result, type 304 stainless steel is stable to be used as a current collector of positive electrode for lithium-ion batteries, similar to Al. No formation of stainless steel – Li alloy is also desirable to employ the stainless steel as a current collector of negative electrode and cell cases for lithium-ion batteries.

## *4. Conclusions*

The electrochemical stability of type 304 stainless steel in a non-aqueous



Accepted Manuscript

ACCEPTED MANUSCRIPT

solution, 1M $LiPF_6$ in EC-DEC (1:1 v/v), was examined. The stainless steel passivated well up to 5 V vs. $Li/Li^+$ in the electrolytic system. As elucidated by ToF-SIMS, the passive layer was composed of (Cr, Fe)-oxides, on which (Cr, Fe)-fluorides resided. Passivation accomplished by the (Cr, Fe)-fluorides layer would contribute to improved corrosion resistance compared to the oxides layer in the alkyl carbonate solution that is commonly employed as an electrolyte for lithium-ion batteries. This property would give further possibilities that type 304 stainless steel (thin foil) can be applicable as current collectors for both positive and negative electrodes, and cell cases for lithium-ion batteries.

## *5. References*

[1] H. H. Uhlig, S. S. Lord, Jr., *J. Electrochem. Soc.*, **100** (1953) 216.

[2] H. H. Uhlig, A. Geary, *J. Electrochem. Soc.*, **101** (1954) 215.

[3] H. P. Leckie, H. H. Uhlig, *J. Electrochem. Soc.*, **113** (1966) 1262.

[4] C. Iwakura, Y. Fukumoto, H. Inoue, S. Ohashi, S. Kobayashi, H. Tada, M. Abe, *J. Power Sources*, **68** (1997) 301.

[5] K. Kanamura, T. Umegaki, S. Shiraishi, M. Ohashi, Z.-I. Takehara, *J. Electrochem. Soc.*, **149** (2002) A185.



Accepted Manuscript

ACCEPTED MANUSCRIPT

[6] J. W. Braithwaite, A. Gonzales, G. Nagasubramanian, S. J. Lucero, D. E. Peebles, J. A. Ohlhausen, W. R. Cieslak, *J. Electrochem. Soc.*, **146** (1999) 488.

[7] S. S. Zhang, K. Xu, T. R. Jow, *J. Electrochem. Soc.*, **149** (2002) A586.

[8] E. Heitz, *Advances in Corrosion Science and Technology*, Edited by M. Fontana, R. Staehle, Vol. 4, p. 149, Plenum Press, New York (1974).

[9] R. G. Kelly, P. J. Moran, C. Zollman, E. Gileadi, J. Kurger, *J. Electrochem. Soc.*, **136** (1989)3262.

[10] R. G. Kelly, P. J. Moran, E. Gileadi, J. Kurger, *Electrochim. Acta*, **34** (1989) 823.

[11] D. A. Shifler, P. J. Moran, J. Kruger, *Corrosion Science*, **32** (1991) 475.

[12] D. A. Shifler, P. J. Moran, J. Kruger, *J. Electrochem. Soc.*, **139** (1992) 54.

[13] S. Komaba, N. Kumagai, M. Baba, F. Miura, N. Fujita, H. Groult, D. Devilliers, B. Kaplan, *J. Appl. Electrochem.*, **30** (2000) 1179.

[14] C. D. Wagner, W. M. Riggs, L. E. Davis, J. F. Moulder, *Handbook of X-ray Photoelectron Spectroscopy*, Perkin Elmer Corp., Physics and Electronics Division, Eden Prairie, MN, 1979.

[15] D. Aurbach, M. D. Levi, E. Levi, A. Schechter, *J. Phys. Chem. B,* **101** (1997) 2195.

[16] *NBS Tables of Chemical Thermodynamic Properties*, J. Phys. Chem. Ref. Data 11



Accepted Manuscript

ACCEPTED MANUSCRIPT

(suppl. 2) (1982).

[17] M. Pourbaix, *Atlas of Electrochemical Equilibria in Aqueous Solutions*, 2nd Ed., NACE (1974).

[18] J.-T. Li, V. Maurice, J. Swiatowska-Mrowiecka, A. Seyeux, S. Zanna, L. Klein, S.-G. Sun, P. Marcus, *Electrochim. Acta*, doi:10.1016/j.electacta.2009.01.052.

[19] D. Aurbach, *J. Electrochem. Soc.*, **136** (1989) 906.

[20] K. Edstrom, T. Gustafsson, J.O. Thomas, *Electrochim. Acta*, **50** (2004) 397.

[21] S.-T. Myung, K. Izumi, S. Komaba, Y.-K. Sun, H. Yashiro, N. Kumagai, *Chem. Mater.*, **17** (2005) 3695.

[22] S.-T. Myung, K. Hosoya, S. Komaba, H. Yashiro, Y.-K. Sun, N. Kumagai, *Electrochim. Acta*, **51** (2007) 5912.

[23] S.-T. Myung, K. Izumi, S. Komaba, H. Yashiro, H. J. Bang, Y.-K. Sun, N. Kumagai, *J. Phys. Chem. C*, **111** (2007) 4061.

[24] Y.-K. Sun, J.-M. Han, S.-T. Myung, S.-W. Lee, K. Amine, *Electrochem. Commun.*, **8** (2006) 821.

[25] Y.-K. Sun, S.-T. Myung, B.-C. Park, H. Yashiro, *J. Electrochem. Soc.*, **155** (2008) A705.

[26] J.-M. Han, S.-T. Myung, Y.-K. Sun, *J. Electrochem. Soc.*, **153** (2006) A1290.



Accepted Manuscript

ACCEPTED MANUSCRIPT

[27] K.-S. Lee, S.-T. Myung, K. Amine, H. Yashiro, Y.-K. Sun, *J. Mater. Chem.*, 19 (2009) 1995.

Accepted Manuscript

ACCEPTED MANUSCRIPT

## *Figure captions*

**Figure 1.** Schematic drawing of the electrochemical cell for the scratch test.

**Figure 2.** Three consecutive cyclic voltamogramms of type 304 stainless steel. Scanning started from OCP in the cathodic direction with a sweeping rate of 10 mV $sec^{-1}$ at 40 $^{o}$C.

**Figure 3.** XPS spectra of (a) Fe2p and (b) Cr2p for type 304 stainless steel after the cathodic polarization at 0 V vs. $Li/Li^{+}$.

**Figure 4.** Time and current (*i*-*t*) curves of the stainless steel after scratching tests at 3 V, 4 V, and 5 V vs. $Li/Li^{+}$.

**Figure 5.** (a) optical microscopic image, (b) total secondary-ion mapping image, (c) ToF-SIMS fragments of as-received, (d) after $Ga^{+}$ ion beam etching for 10s, (e) 30s, (f) 100s, and (g) 1000s after scratch test at 3 V vs. $Li/Li^{+}$. Scale bar indicates 100 μm.

**Figure 6.** (a) optical microscopic image, (b) total secondary-ion mapping image, (c) ToF-SIMS fragments of as-received, (d) after $Ga^{+}$ ion beam etching for 10s, (e) 30s, (f) 100s, and (g) 1000s after scratch test at 4 V vs. $Li/Li^{+}$. Scale bar indicates 100 μm.

**Figure 7.** (a) optical microscopic image, (b) total secondary-ion mapping image, (c) ToF-SIMS fragments of as-received, (d) after $Ga^{+}$ ion beam etching for 10s, (e) 30s, (f) 100s, and (g) 1000s. After scratch test at 5 V vs. $Li/Li^{+}$. Scale bar indicates 100 μm.

**Figure 8.** Comparison of the relative intensities of fragments: (a) after scratch test at 4 V vs. $Li/Li^{+}$ and (b) at 5 V vs. $Li/Li^{+}$.

**Figure 9.** Schematic drawing of the passivation process for type 304 stainless steel in the non-aqueous alkyl carbonate solution containing $LiPF_6$ salt.



Accepted Manuscript

ACCEPTED MANUSCRIPT

Table 1. The nominal chemical composition of type 304 stainless steel (mass %).

| | C | Si | Mn | Ni | Cr | Fe |
|---|---|---|---|---|---|---|
| Type 304 | < 0.08 | < 1 | < 2 | 8 - 11 | 18 - 20 | Balance |

Accepted Manuscript

ACCEPTED MANUSCRIPT

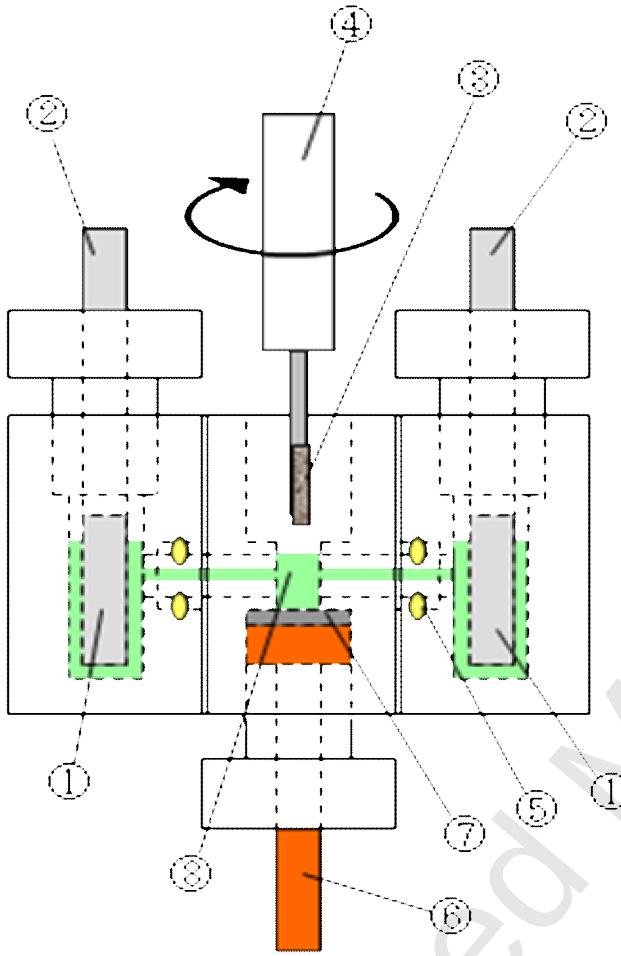


1. Li metal
2. Ni tab
3. Diamond polishing tip
4. PTFE impeller
5. O-ring
6. Cu rod
7. Stainless steel working electrode

**Figure 1.** Schematic drawing of the electrochemical cell for the scratch test.

Accepted Manuscript

ACCEPTED MANUSCRIPT

**Figure 2.** Three consecutive cyclic voltamogramms of type 304 stainless steel. Scanning started from OCP in the cathodic direction with a sweeping rate of 10 mV $sec^{-1}$ at 40 $^{o}$C.

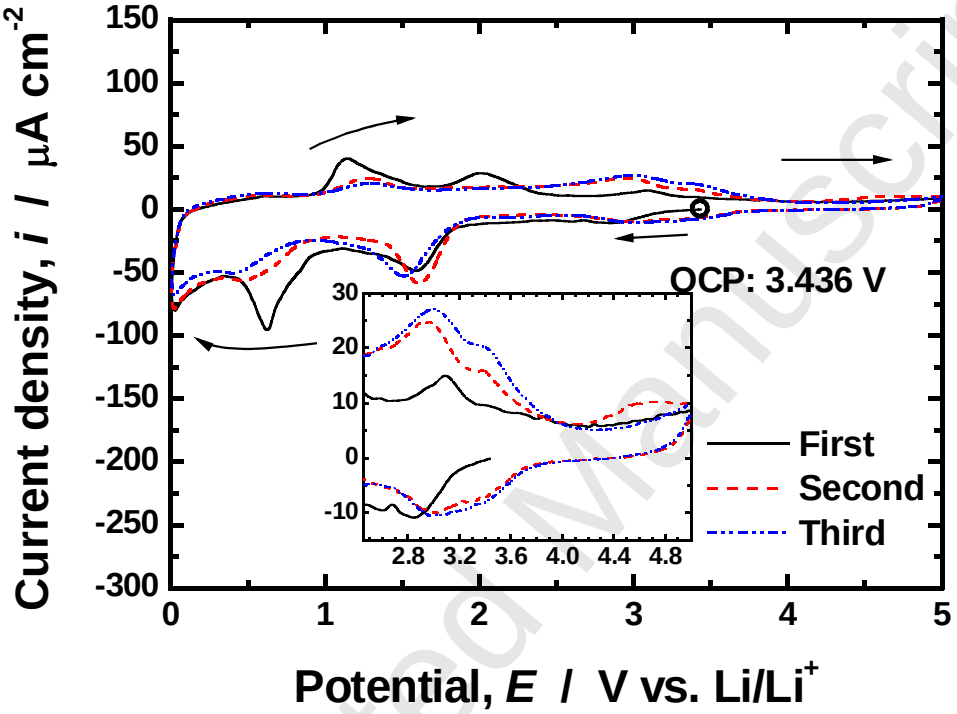


Accepted Manuscript

ACCEPTED MANUSCRIPT

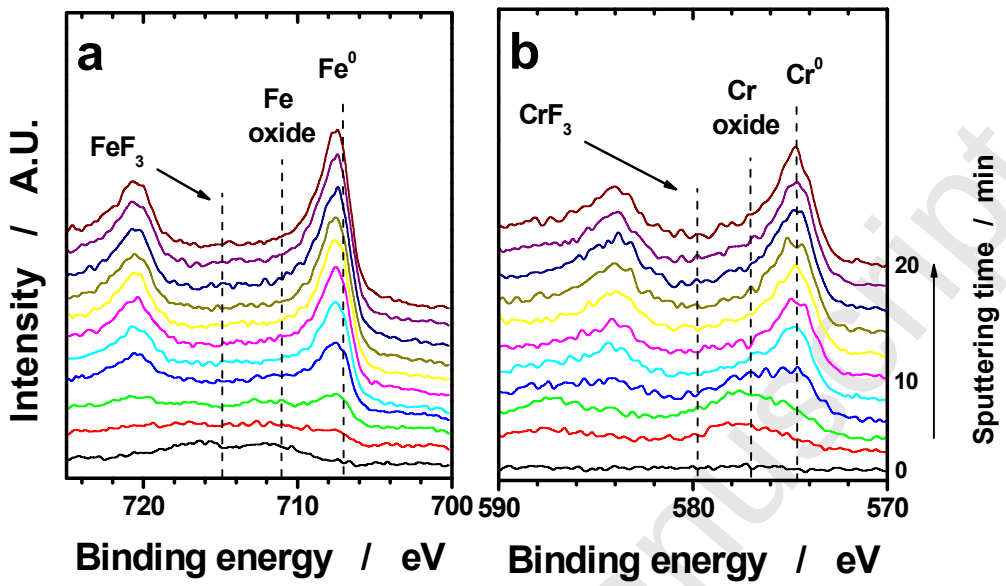


**Figure 3.** XPS spectra of (a) Fe2p and (b) Cr2p for type 304 stainless steel after the cathodic polarization at 0 V vs. $Li/Li^+$.

Accepted Manuscript

ACCEPTED MANUSCRIPT

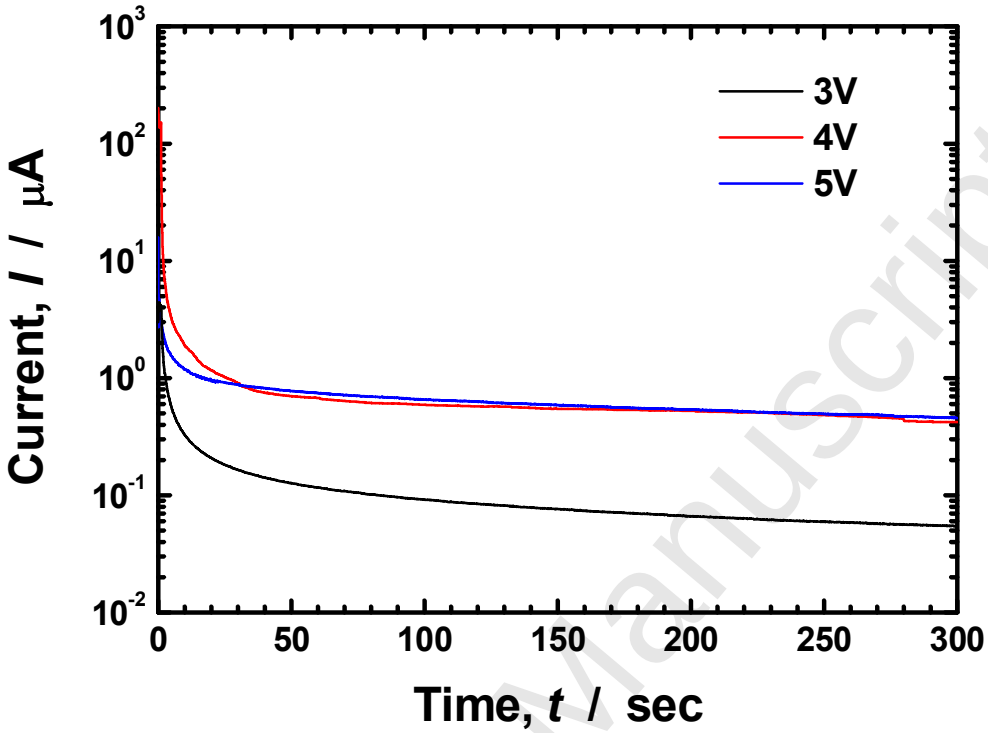


**Figure 4.** Time and current (*i*-*t*) curves of the stainless steel after scratching tests at 3 V, 4 V, and 5 V vs. $Li/Li^+$.

Accepted Manuscript

ACCEPTED MANUSCRIPT

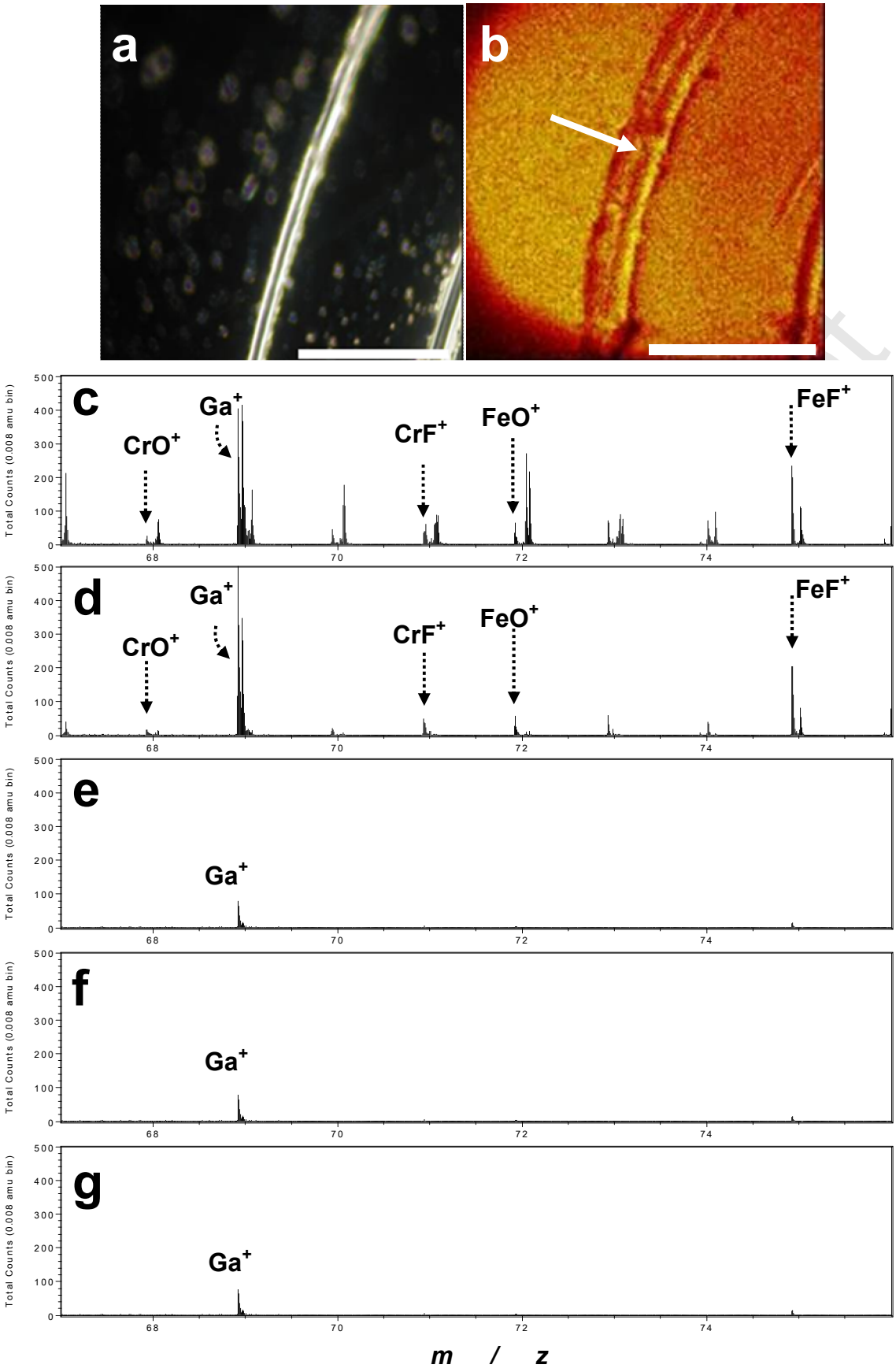


**Figure 5.** (a) optical microscopic image, (b) total secondary-ion mapping image, (c) ToF-SIMS fragments of as-received, (d) after $Ga^+$ ion beam etching for 10s, (e) 30s, (f) 100s, and (g) 1000s after scratch test at 3 V vs. $Li/Li^+$. Scale bar indicates 100 μm.

ACCEPTED MANUSCRIPT

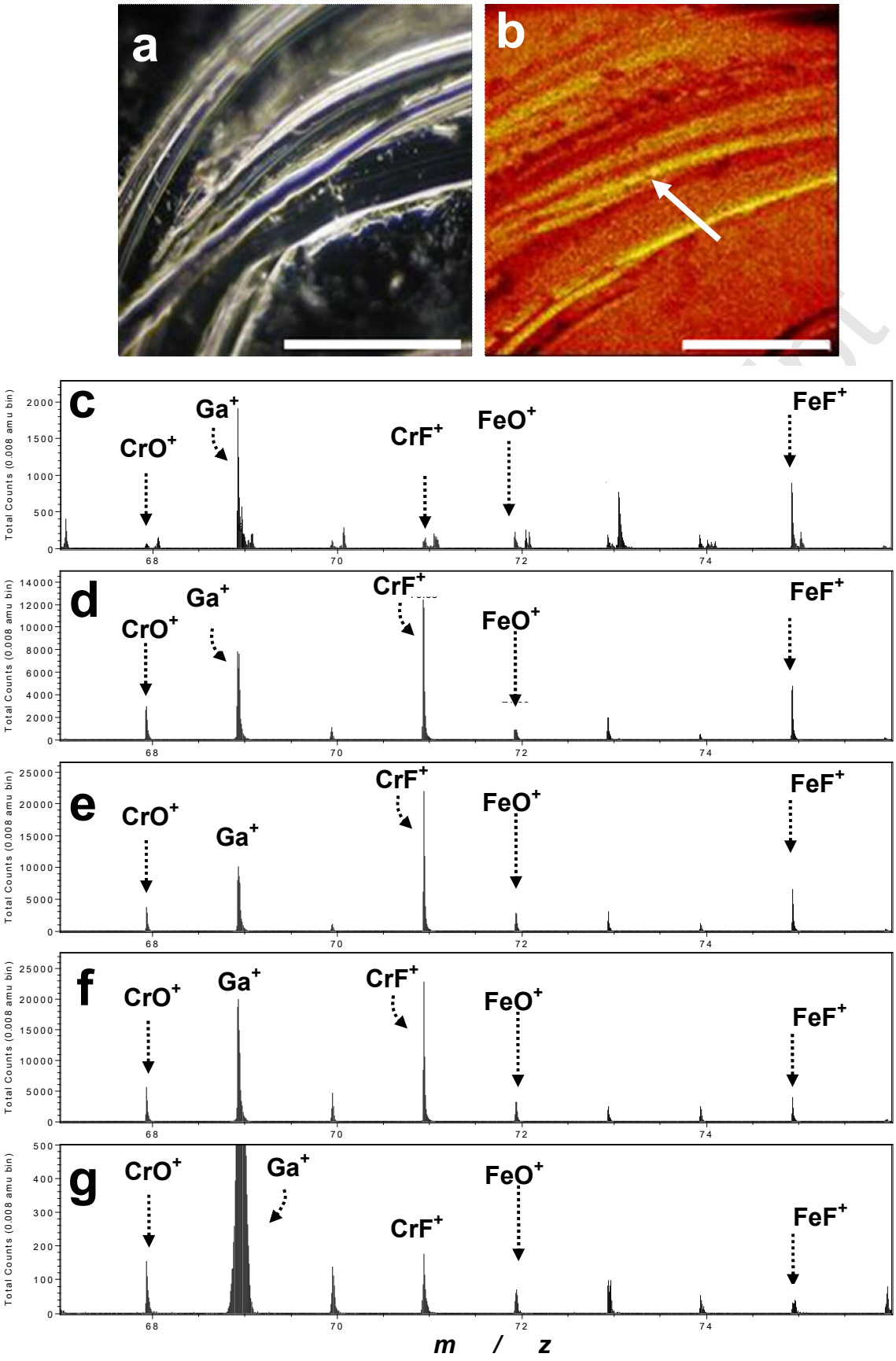


**Figure 6.** (a) optical microscopic image, (b) total secondary-ion mapping image, (c) ToF-SIMS fragments of as-received, (d) after $Ga^+$ ion beam etching for 10s, (e) 30s, (f) 100s, and (g) 1000s after scratch test at 4 V vs. $Li/Li^+$. Scale bar indicates 100 μm.

ACCEPTED MANUSCRIPT

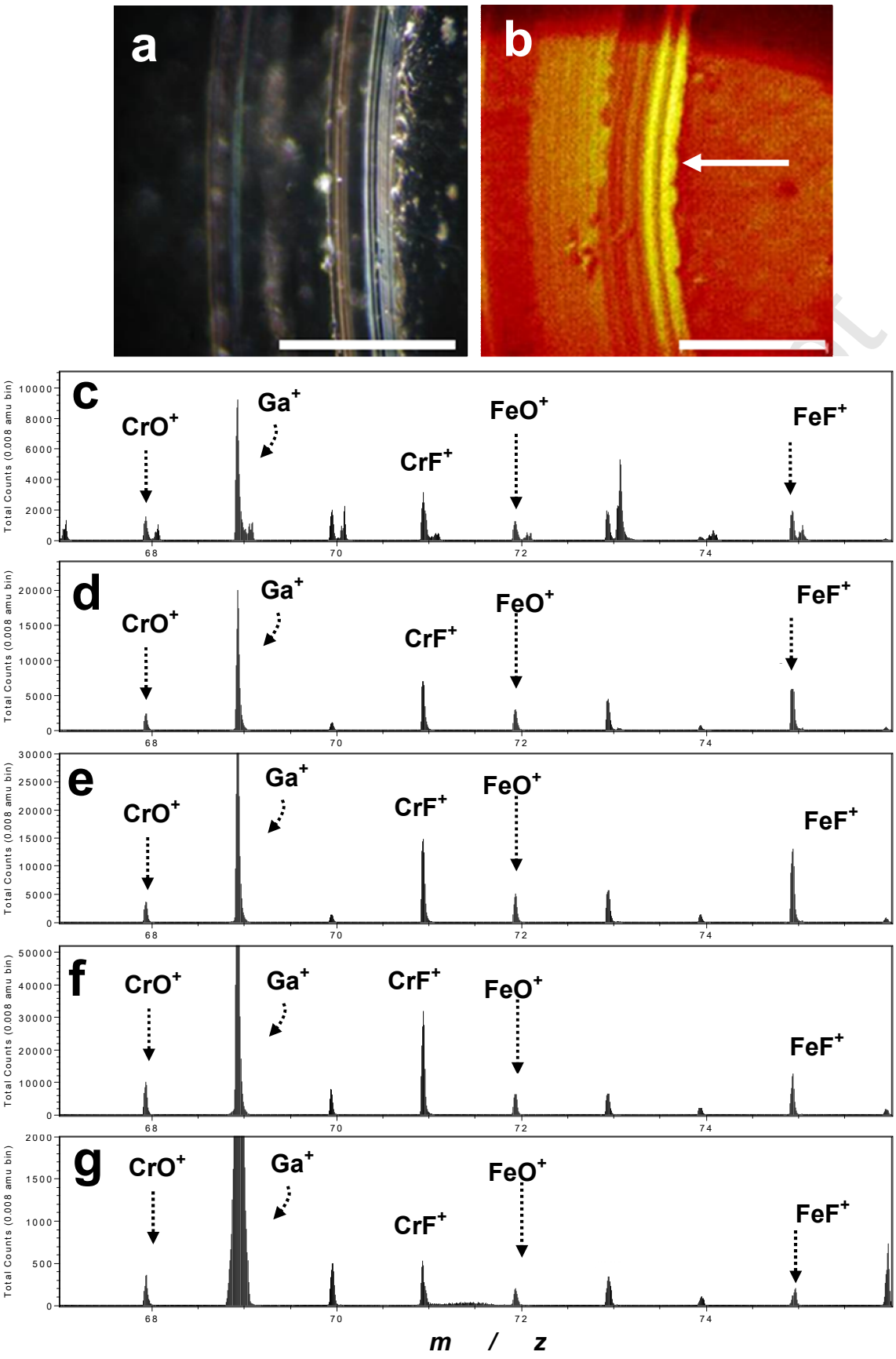


**Figure 7.** (a) optical microscopic image, (b) total secondary-ion mapping image, (c) ToF-SIMS fragments of as-received, (d) after $Ga^+$ ion beam etching for 10s, (e) 30s, (f) 100s, and (g) 1000s. After scratch test at 5 V vs. $Li/Li^+$. Scale bar indicates 100 μm.

ACCEPTED MANUSCRIPT

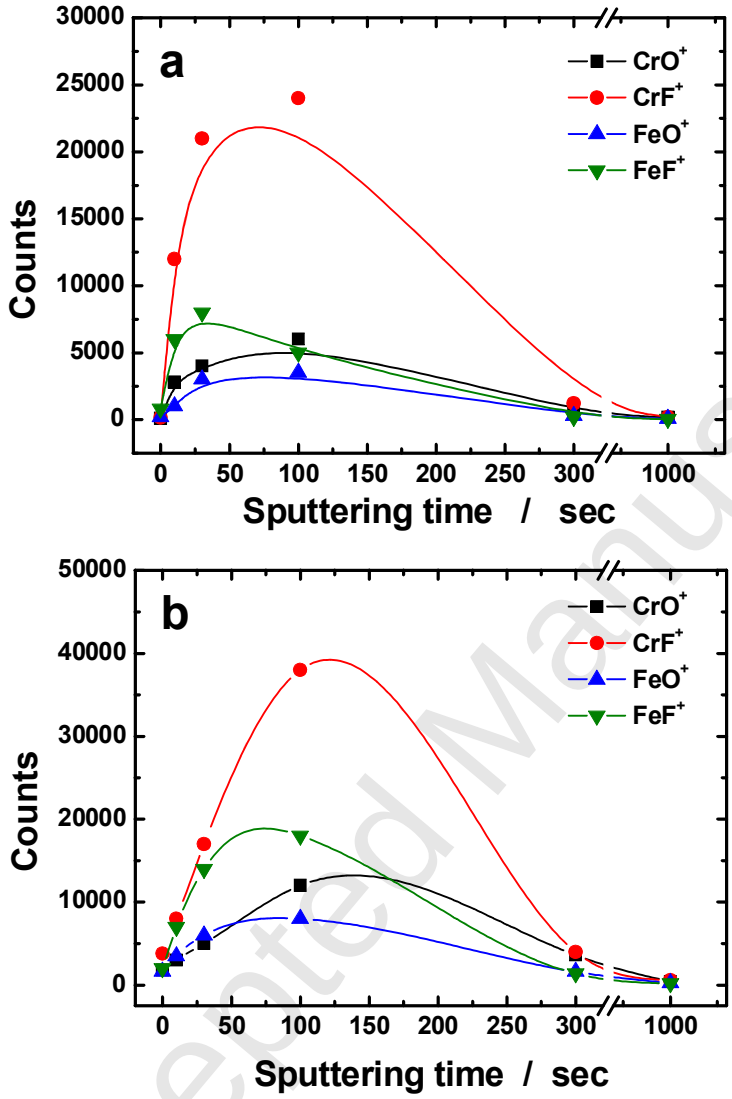


**Figure 8.** Comparison of the relative intensities of fragments: (a) after scratch test at 4 V vs. $Li/Li^+$ and (b) at 5 V vs. $Li/Li^+$.

Accepted Manuscript

ACCEPTED MANUSCRIPT

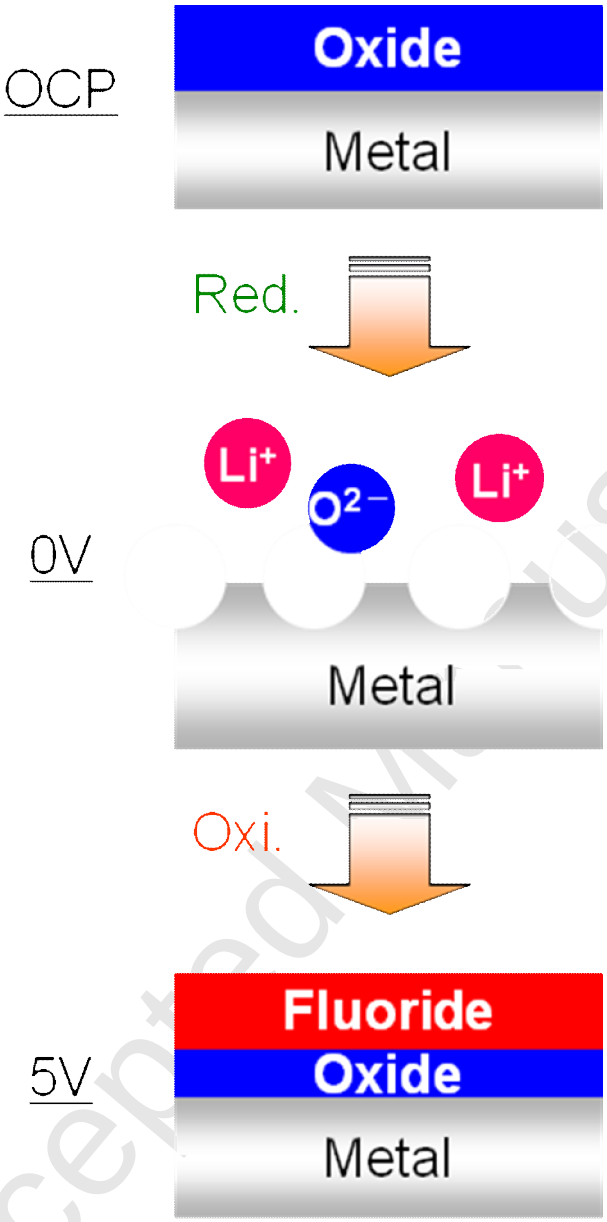


**Figure 9.** Schematic drawing of the passivation process for type 304 stainless steel in the non-aqueous alkyl carbonate solution containing $LiPF_6$ salt.

Accepted Manuscript